THE JOURNAL OF PHYSICAL CHEMISTRY Letters

Letter

pubs.acs.org/JPCL

Size Effects in the Interface Level Alignment of Dye-Sensitized TiO_2 Clusters

Noa Marom,*[,†,‡] Thomas Körzdörfer,[§] Xinguo Ren,[∥] Alexandre Tkatchenko,[⊥] and James R. Chelikowsky[‡]

[†]Physics and Engineering Physics, Tulane University, New Orleans, Louisiana 70118, United States

[‡]Institute for Computational Engineering and Sciences (ICES), The University of Texas at Austin, Austin, Texas 78712, United States

[§]Computational Chemistry, University of Potsdam, 14476 Potsdam, Germany

[∥]Key Laboratory of Quantum Information, University of Science and Technology of China, Hefei, Anhui 230026, China

[⊥]Fritz-Haber-Institut der Max-Planck-Gesellschaft, Faradayweg 4-6, 14195, Berlin, Germany

Supporting Information

ABSTRACT: The efficiency of dye-sensitized solar cells (DSCs) depends critically on the electronic structure of the interfaces in the active region. We employ recently developed dispersion-inclusive density functional theory (DFT) and GW methods to study the electronic structure of TiO_2 clusters sensitized with catechol molecules. We show that the energy level alignment at the dye-TiO_2 interface is the result of an intricate interplay of quantum size effects and dynamic screening effects and that it may be manipulated by nanostructuring and functionalizing the TiO_2. We demonstrate that the energy difference between the catechol LUMO and the TiO_2 LUMO, which is associated with the injection loss in DSCs, may be reduced significantly by reducing the dimensions of nanostructured TiO_2 and by functionalizing the TiO_2 with wide-gap moieties, which contribute additional screening but do not interact strongly with the frontier orbitals of the TiO_2 and the dye. Precise control of the electronic structure may be achieved via "interface engineering" in functional nanostructures.

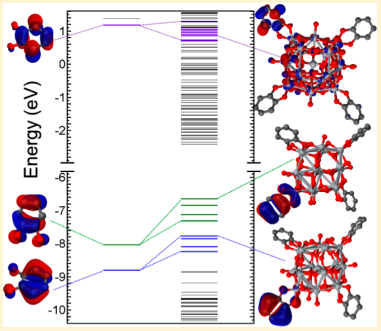

SECTION: Molecular Structure, Quantum Chemistry, and General Theory

Nobel laureate Herbert Kroemer coined the phrase "the interface is the device".[1] This is certainly true for dye-sensitized solar cells (DSCs).[2−5] DSCs are hybrid organic−inorganic systems. As such, they enjoy the best of both worlds by combining the high charge carrier mobility and efficient electrical charge injection of the inorganic component with the strong light-matter coupling and rich chemical compound space of the organic component. In DSCs, sunlight is harvested by (metal-) organic dyes, attached to a nanostructured oxide, typically TiO_2. Charge separation is achieved at the dye−oxide interface via electron injection from the lowest unoccupied molecular orbital (LUMO) of the dye into the conduction band of the oxide. Regeneration occurs via hole transfer from the highest occupied molecular orbital (HOMO) of the dye to a hole conductor (often, a redox pair in solution). The energy differences between the dye LUMO (HOMO) and the oxide conduction band edge (redox potential) provide the driving force for injection (regeneration). These unavoidable injection and regeneration losses reduce the maximal open circuit voltage of a DSC. Typically, an energy difference of a fraction of an electron volt at the interface is considered to provide a good balance between the injection (regeneration) efficiency and the voltage loss.[3] Thus, the efficiency of a DSC depends critically on the electronic structure of the interfaces in its active region.

Owing to quantum effects at the nanoscale, the energy level alignment at the interface depends strongly on the local environment and cannot be derived directly from the positions of the energy levels of isolated species. First, the gap of a molecule on a surface narrows with respect to its gas phase gap because of screening.[6−14] Second, the electronic properties of nanostructured TiO_2 depend strongly on size and structure.[15−18] Third, the orientation of dye molecules with respect to the oxide surface affects the coupling at the interface and may alter the conditions for charge transfer.[19−22] Interfaces in DSCs are typically disordered, and their measured properties, such as the open circuit voltage, must be regarded as an average over several configurations, some of which are better than others. In addition to harboring some less than optimal configurations, disorder may cause losses due to traps and tail states.[23] The incomplete understanding of all the factors affecting the electronic structure and functionality of these interfaces and the lack of clear design rules have led to the perception that disorder is essential, rather than detrimental, to the operation of DSCs because it is on average better than a less than optimal order.

First-principles quantum mechanical simulations enable a systematic investigation of nanostructured interfaces to elucidate the relations between structural configuration and electronic properties and to derive design rules for more efficient DSCs.

Received: April 29, 2014
Accepted: June 19, 2014
Published: June 19, 2014

   dx.doi.org/10.1021/jz5008356 | J. Phys. Chem. Lett. 2014, 5, 2395−2401

The present study focuses on how the energy level alignment at the dye-TiO_2 interface may be manipulated by nanostructuring and functionalizing the TiO_2. It is demonstrated that the interface level alignment is the result of an intricate interplay of quantum size effects and dynamic screening effects. The energy difference between the catechol LUMO and the TiO_2 LUMO, which is associated with the injection loss, may be reduced significantly by reducing the dimensions of nanostructured TiO_2 and by functionalizing the TiO_2 with wide-gap moieties, which contribute additional screening but do not interact strongly with the frontier orbitals of the TiO_2 and the dye. Precise control of the electronic structure may be achieved via "interface engineering".

We examine three of the crystalline nanocluster phases synthesized by Benedict and Coppens,[24] shown in Figure 1.

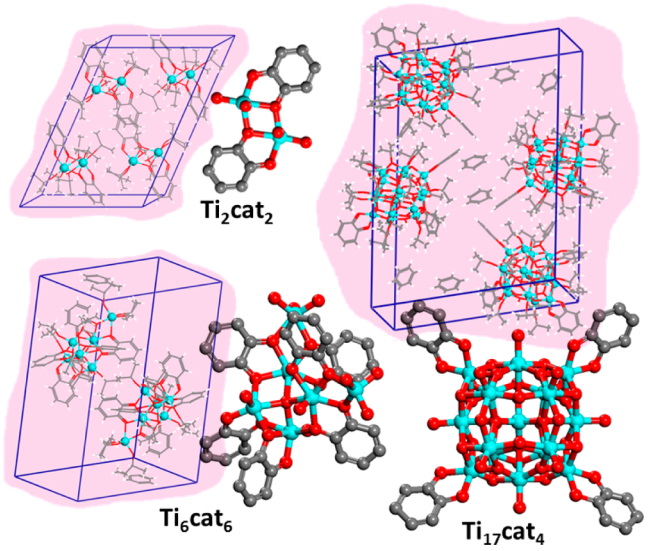

Figure 1. Illustrations of the unit cells of the crystalline phases of TiO_2 clusters sensitized with catechol from ref 24 and of the reduced structures without the isopropoxy (IPr) moieties (hydrogen atoms are not shown for clarity). Ti_2cat_2, Ti_6cat_6, and $Ti_{17}cat_4$ comprise TiO_2 clusters with 2, 6, and 17 Ti atoms, functionalized with 2, 6, and 4 catechol (cat) molecules, respectively. Ti atoms are colored in cyan, O atoms in red, C atoms in gray, and H atoms in white.

They comprise TiO_2 clusters of increasing size, functionalized with catechol (cat) molecules, and terminated with isopropoxy (IPr) moieties, such that the Ti atoms are 6-coordinated. Ti_2cat_2, Ti_6cat_6, and $Ti_{17}cat_4$ comprise 2, 6, and 17 Ti atoms and 2, 6, and 4 catechol molecules, respectively. These systems are useful models for fundamental studies of the dye-TiO_2 interface because they have a well-defined structure, characterized by single crystal X-ray diffraction (XRD). In ref 25, the interface level alignment of Ti_2cat_2 was compared to that of a system comprising a TiO_2 cluster of a similar size functionalized with isonicotinic acid (INA). Here, it is compared to systems comprising larger TiO_2 clusters to investigate size effects. The catechol molecule and the TiO_2 clusters studied here are much smaller than the dyes and TiO_2 particles typically used in DSCs, which makes them amenable to high accuracy ab initio simulations.

All calculations were performed with the all-electron numerical atom-centered orbital (NAO) code, FHI-aims[26−28] using *tier 2* basis sets. In ref 25, the internal parameters of the Ti_2cat_2 unit cell (376 atoms) were relaxed using dispersion-inclusive density functional theory (DFT) with the Perdew−Burke−Ernzerhof (PBE)[29,30] exchange-correlation functional and the Tkatchenko-Scheffler (TS)[31] dispersion method. It was shown that the atomic positions obtained with PBE+TS overlapped with the XRD structure almost exactly. Here, owing to the size of the Ti_6cat_6, and $Ti_{17}cat_4$ unit cells (408 and 1172 atoms, respectively) only the hydrogen positions were relaxed because these are determined less accurately by XRD. For $Ti_{17}cat_4$ hydrogen positions were not reported in ref 24. The structure of the unit cell with relaxed hydrogen positions is provided in the Supporting Information. We note that H atoms were added on four bridging oxygen sites, which otherwise produce gap states.

An accurate description of the fundamental gaps and the level alignment at interfaces calls for a treatment beyond ground state DFT. Here, we employ many-body perturbation theory within the GW approximation.[32−34] In this approximation, the self-energy is obtained from the product of the one-particle Green's function, G, and the dynamically screened Coulomb interaction, W. Owing to the computational cost of fully self-consistent GW calculations, a perturbative approach, known as G_0W_0, is typically used. The quasi-particle (QP) excitation energies are obtained as a first-order correction to the DFT eigenvalues. G and W are evaluated using the underlying Kohn−Sham (KS) orbitals. The G_0W_0 scheme has had some notable success in the description of the electronic structure of organic−inorganic interfaces, including dye−TiO_2 interfaces.[6−14,25] In particular, G_0W_0 captures the polarization-induced renormalization of the molecular energy levels at the interface, a dynamic correlation effect inherently absent from standard DFT functionals.

To study the catechol−TiO_2 interface, nonperiodic G_0W_0 calculations were performed for the reduced model systems, shown in Figure 1. The IPr moieties were removed, keeping only the oxygen atoms to maintain the Ti coordination. Dangling bonds were passivated with hydrogen (following the procedure of ref 25.). The effect of functionalization with IPr was studied for Ti_2cat_2 and Ti_6cat_6 ($Ti_{17}cat_4$, with 269 atoms, was too large for G_0W_0 calculations). Owing to the size of some of the systems studied here, G_0W_0 calculations were performed with *tier 2* basis sets. It has been demonstrated in ref 35 that, at the *tier 2* level, G_0W_0 spectra are already converged in terms of the ordering and energy differences of the orbitals. The difference between G_0W_0 spectra obtained with *tier 2* basis sets and the more converged *tier 4* basis sets typically amounts to a rigid shift of the whole spectrum by about 0.2 eV. A comparison between the *tier 2* and *tier 4* basis sets for the spectrum of catechol is provided as Supporting Information.

The fact that G_0W_0 QP energies are calculated non-self-consistently gives rise to a strong dependence on the DFT starting point. This is of particular importance when semilocal DFT functionals yield a qualitatively incorrect picture.[36−42] Self-interaction errors (SIE), the spurious interaction of an electron with itself,[43] often render semilocal DFT inadequate as a starting point for G_0W_0. SIE may cause qualitative changes in the ordering of frontier molecular orbitals because the spurious Coulomb repulsion destabilizes localized orbitals with respect to delocalized orbitals.[44−46] This effect of SIE propagates from the DFT level to the G_0W_0 level. The inclusion of a fraction of exact exchange (EXX) in hybrid functionals mitigates SIE and provides a better starting point for G_0W_0 calculations.[25,28,35,47−49] It has been shown that G_0W_0 based on a good mean-field starting point may outperform GW methods at a higher level of self-consistency, owing to error cancellation between the underscreening resulting from neglecting the

dx.doi.org/10.1021/jz5008356 | J. Phys. Chem. Lett. 2014, 5, 2395−2401

vertex and the overscreening produced by DFT functionals.[35] We note that in some cases, in particular if orbital rehybridization occurs at the interface, some form of self-consistency in the wave function may be required.[13,14,25] For the systems studied here, no such rehybridization is found, and the G_0W_0 approximation remains valid.

We employ a recently developed first-principles method for finding a consistent starting point (CSP) for G_0W_0.[50] This is achieved by optimizing the fraction of EXX in a global hybrid functional within the framework of generalized Kohn−Sham (GKS) theory. Using a hybrid functional starting point, the G_0W_0 QP energies, $\varepsilon_i^{G_0W_0}$, are given as follows:

$$\begin{aligned}\varepsilon_i^{G_0W_0} &= \varepsilon_i^{GKS} + (1 - b_{HF})\langle\varphi_i(r)|\hat{v}_x^{HF} - v_x^{KS}[n]|\varphi_i(r)\rangle \\ &\quad + \langle\varphi_i(r)|\hat{\Sigma}_c - v_c^{KS}[n]|\varphi_i(r)\rangle \\ &=: \varepsilon_i^{GKS} + (1 - b_{HF})\Delta v_{x,i} + \Delta v_{c,i}\end{aligned} \tag{1}$$

where $\varphi_i(r)$ and ε_i^{KS} are the ith DFT orbital and eigenvalue, respectively, $\hat{v}_x^{HF}$ is the nonlocal Hartree−Fock (HF) exchange operator, $\hat{\Sigma}_c$ is the G_0W_0 correlation self-energy, $v_x^{KS}[n]$ and $v_c^{KS}[n]$ are the semilocal exchange and correlation potentials, respectively, and b_{HF} is the fraction of EXX. For orbital i, the difference between the HF and semilocal exchange energy is denoted as $\Delta v_{x,i}$ and the difference between the G_0W_0 and semilocal correlation energy is denoted as $\Delta v_{c,i}$. If a fraction of EXX can be found, such that for all orbitals:

$$(1 - b_{HF})\Delta v_{x,i} + \Delta v_{c,i} \approx \text{const} \tag{2}$$

then the resulting DFT eigenvalue spectrum may be considered consistent with the G_0W_0 spectrum in the sense that the relative orbital energies are correct and the QP correction amounts to a rigid shift of the entire spectrum. This is the essential feature of the CSP, derived in ref 50. The fraction of EXX in the CSP is extracted from the slope of a linear fit of $\Delta v_{c,i}$ as a function of $\Delta v_{x,i}$. Such plots for the systems studied here are provided in the Supporting Information. G_0W_0@CSP has been shown to yield QP spectra in excellent agreement with photoemission spectroscopy (PES) experiments for various organic semiconductors.[50] The fractions of EXX in a PBE-based hybrid CSP for the systems studied here are shown in Table 1.[51]

Table 1. Fraction of Exact Exchange in the Consistent Starting Point (CSP) Used for G_0W_0 Calculations of the Systems Studied Here

system	CSP	system	CSP
catechol	0.28	$Ti_{17}cat_4$ w/o IPr	0.26
Ti_2cat_2 w/o IPr	0.29	Ti_2cat_2	0.20
Ti_6cat_6 w/o IPr	0.26	Ti_6cat_6	0.19

Figure 2 shows G_0W_0@CSP energy level diagrams for Ti_2cat_2, Ti_6cat_6, and $Ti_{17}cat_4$ without the IPr moieties, as well as illustrations of the frontier orbitals. The orbitals associated with the HOMO, HOMO−1, and LUMO of catechol and the orbitals associated with the TiO_2 clusters may be identified by visual inspection. For all three systems, the catechol HOMO and HOMO−1 lie in the gap of the TiO_2 clusters. The catechol LUMO lies in the empty state manifold of the TiO_2 clusters and is strongly hybridized with TiO_2 states. Such strong coupling between the dye LUMO and the oxide is considered favorable for electron injection. Although the three systems share some qualitative similarity, they differ in the quantitative details of the energy level alignment at the interface.

Owing to quantum size effects, the fundamental gap of the TiO_2 clusters (denoted by red arrows) narrows with increasing cluster size from 9.2 eV for the smallest cluster with 2 Ti atoms to 6.4 eV for the largest cluster with 17 Ti atoms. This is still significantly larger than the reported bulk GW gaps of 3.38−3.78 eV for rutile[14,52−54] and 3.79−3.83 eV for anatase[52,55] TiO_2.[56] This demonstrates that the band edges of TiO_2 may be tuned within a range of several eV by nanostructuring. At the same time, the screening produced by the TiO_2 clusters also increases with size. This enhances the polarization induced gap narrowing effect, such that the gap of the catechol molecule (denoted by light blue arrows) narrows from 9.4 eV in the gas phase to 8.4 eV when attached to the smallest TiO_2 cluster and to 7.4 eV when attached to the largest TiO_2 cluster.

The combination of quantum size effects and polarization induced gap narrowing leads to simultaneous reduction of the gaps of the TiO_2 clusters and of the catechol molecules attached to them. The gap of the TiO_2 clusters narrows faster with system size than the gap of catechol. In addition, rather than affecting both sides of the gap equally, screening affects the position of the catechol HOMO more strongly, while quantum confinement affects the position of the TiO_2 LUMO more strongly. As a result, the energy level alignment at the interface changes in an unintuitive way. The energy difference between the highest state associated with the catechol HOMO and the TiO_2 cluster HOMO (denoted by pink arrows) decreases from 2.8 eV for the smallest system to 2.2 eV for the largest system. More important is the change in the energy difference between the lowest state associated with the catechol LUMO and the TiO_2 cluster LUMO (denoted by light green arrows), which grows from 2.0 eV for the smallest system to 3.1 eV for the largest system. This demonstrates that the injection loss may be reduced significantly by reducing the dimensions of nanostructured TiO_2.

Figure 3 shows G_0W_0@CSP energy level diagrams for Ti_2cat_2 and Ti_6cat_6 (with the IPr moieties) and illustrations of the frontier orbitals. As reported in ref 25 for similar systems, the IPr moieties do not change the qualitative picture of the alignment between the frontier orbitals of catechol and those of the TiO_2 clusters. The HOMO of IPr hybridizes with the HOMO−2 of catechol and some valence states of the TiO_2 clusters. The main effect of the IPr moieties is to contribute additional screening. This leads to narrowing of the TiO_2 and catechol gaps and to a decrease in the energy differences between the highest orbital associated with the catechol HOMO and the TiO_2 HOMO and between the lowest orbital associated with the catechol LUMO and the TiO_2 LUMO. The latter demonstrates that functionalizing the TiO_2 may alter the level alignment at the interface to reduce the injection loss (capping moieties may offer the additional benefit of eliminating surface states that cause losses).

The crystalline environment is expected to enhance the screening and further reduce the gaps of the dye-sensitized TiO_2 clusters. To estimate the magnitude of this effect we use an electrostatic model for the polarization energy. P is the stabilization energy of an ionized molecule due to screening by the surrounding molecules in a solid.[57,58] The gap narrows by $2P$ because the ionization potential is decreased by P while the

dx.doi.org/10.1021/jz5008356 | J. Phys. Chem. Lett. 2014, 5, 2395−2401

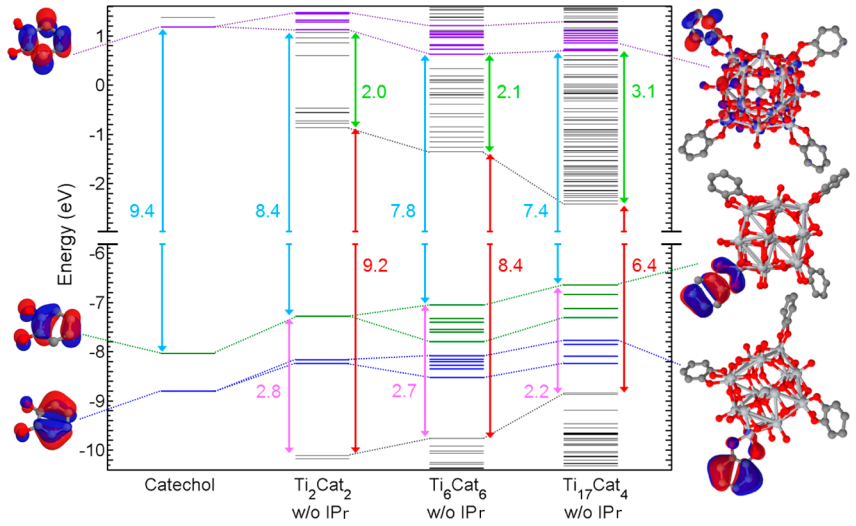

Figure 2. Size effects in the interface level alignment between catechol and increasingly large TiO_2 clusters. Red arrows indicate the cluster gap, light blue arrows indicate the catechol gap, pink arrows indicate the alignment between the catechol HOMO and the cluster's valence states, and light green arrows indicate the alignment between the catechol LUMO and the cluster's unoccupied states. All numbers are in eV. Illustrations of the frontier orbitals are also shown.

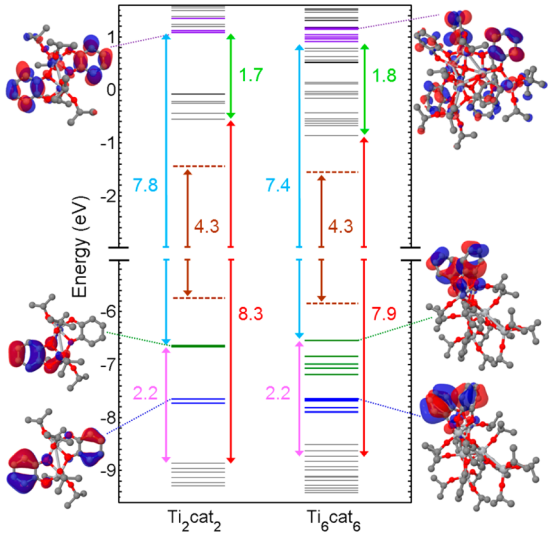

Figure 3. Interface-level alignment of Ti_2cat_2 and Ti_6cat_6. Red arrows indicate the cluster gap, light blue arrows indicate the catechol gap, pink arrows indicate the alignment between the catechol HOMO and the cluster's valence states, light green arrows indicate the alignment between the catechol LUMO and the cluster's unoccupied states, brown dashed lines indicate the narrowing of the gap due to polarization, and brown arrows indicate the gap of the crystalline phases of Ti_2cat_2 and Ti_6cat_6, estimated from the polarization model. All numbers are in eV. Illustrations of the frontier orbitals are also shown.

electron affinity is increased by P. P is given in atomic units by

$$P = -e^2\frac{\varepsilon - 1}{2R\varepsilon} \tag{3}$$

where e is the electron charge, ε is the dielectric constant, and R is the effective volume per molecule in the unit cell, given by

$$R = \left(\frac{3V}{4\pi N}\right)^{1/3} \tag{4}$$

where V is the unit cell volume and N is the number of molecules in the cell. The dielectric constant is obtained from the Clausius–Mossotti relation:

$$\frac{\varepsilon - 1}{\varepsilon + 2} = \frac{4\pi}{3V}\alpha \tag{5}$$

where α is the static polarizability. An accurate description of the polarizability, taking into account long-range screening effects, is provided within the many-body dispersion (MBD)[59] method by solving the Dyson-like self-consistent screening (SCS) equation from classical electrodynamics:

$$\alpha^{\mathrm{SCS}}(\mathbf{r};\, i\omega) = \alpha^{\mathrm{TS}}(\mathbf{r};\, i\omega) + \alpha^{\mathrm{TS}}(\mathbf{r};\, i\omega) \times \int \mathrm{d}\mathbf{r}'\, T(\mathbf{r} - \mathbf{r}')\alpha^{\mathrm{SCS}}(\mathbf{r};\, i\omega) \tag{6}$$

This equation relates the TS unscreened polarizability of an atom in a molecule,[31] α^{TS}, to the fully screened polarizability, α^{SCS}, through the dipole–dipole interaction tensor, T. A detailed description of the method is provided in refs 59 and 60. This method has been shown to yield accurate dielectric constants for molecular crystals of polyacenes.[60] For pentacene, applying the polarization model to the G_0W_0@CSP gas phase gap resulted in excellent agreement with periodic G_0W_0 calculations and experimental values for the fundamental gap of the crystal.

The computed dielectric constants and polarization induced gap narrowing of Ti_2cat_2 and Ti_6cat_6 are given in Table 2.

Table 2. Computed Dielectric Constants and Polarization Induced Gap Narrowing for the Systems Studied Here

system	ε	$2P$ (eV)
Ti_2cat_2	3.72	1.78
Ti_6cat_6	4.08	1.38

The estimated gaps of the crystalline Ti_2cat_2 and Ti_6cat_6, obtained from the polarization model, are shown in brown in Figure 3. Applying the polarization model to both systems results in identical gaps of 4.3 eV. This suggests that the screening in the crystalline phase may mask the size effects in this case. We note that the model systems studied here are

dx.doi.org/10.1021/jz5008356 | J. Phys. Chem. Lett. 2014, 5, 2395−2401

smaller than the dyes and TiO_2 particles used in actual DSCs and consequently their gaps are larger.

The optical gaps are expected to be smaller than the fundamental gaps computed here, owing to the exciton binding energy. In addition, an injection mechanism involving a direct charge transfer from the catechol HOMO to the conduction band of TiO_2 has been suggested.[61−68] These phenomena, associated with neutral excitations, may be treated by solving the Bethe-Salpeter equation on top of GW (GW/BSE), which is outside the scope of the present work. The accurate description of the interface level alignment achieved here may provide the foundation for subsequent treatment of optical excitations and injection dynamics.

To summarize, we employed recently developed dispersion-inclusive DFT and GW methods to study the electronic structure of dye-sensitized TiO_2 clusters. We demonstrated that the interface level alignment changes in an unintuitive way, owing to an intricate interplay of quantum size effects and dynamic screening effects. The energy difference between the catechol LUMO and the TiO_2 LUMO, which is associated with the injection loss in DSCs, may be reduced significantly by reducing the dimensions of nanostructured TiO_2 and by functionalizing the TiO_2 with wide-gap moieties, which contribute additional screening but do not interact strongly with the frontier orbitals of the TiO_2 and the dye. We expect our conclusions regarding the manifestation of size effects in the interface level alignment to be relevant to other hybrid organic−inorganic functional nanostructures. We suggest that precise control of the electronic structure of such materials may be achieved via "interface engineering".

■ ASSOCIATED CONTENT

Supporting Information

Crystal structure of $Ti_{17}cat_4$ with hydrogen positions, including passivation of bridging oxygen sites; detailed $\Delta v_{c,i}$ vs $\Delta v_{x,i}$ plots used to find the CSP for the systems studied here; comparison of G_0W_0@CSP spectra of catechol, calculated with *tier 2* and *tier 4* basis sets, to gas phase photoemission spectroscopy. This material is available free of charge via the Internet http://pubs.acs.org.

■ AUTHOR INFORMATION

Corresponding Author

*E-mail: nmarom@tulane.edu.

Author Contributions

The manuscript was written through contributions of all authors. All authors have given approval to the final version of the manuscript.

Notes

The authors declare no competing financial interest.

■ ACKNOWLEDGMENTS

Work at Tulane University was supported by the Louisiana Alliance for Simulation-Guided Materials Applications (LA-SiGMA), funded by the National Science Foundation (NSF) Award #EPS-1003897. Work at UT-Austin was supported by the Department of Energy for work on nanostructures from Grant DE-FG02-06ER46286. We also wish to acknowledge support provided by the Scientific Discovery through the Advanced Computing (SciDAC) program funded by U.S. Department of Energy, Office of Science, Advanced Scientific Computing Research and Basic Energy Sciences under Award Number DESC0008877 on algorithms. Computer time was provided by the National Energy Research Scientific Computing Center (NERSC), which is supported by the Office of Science of the U.S. Department of Energy under Contract DE-AC02-05CH11231.

■ REFERENCES

(1) Kroemer, H. *Nobel Lectures, Physics 1996−2000*; World Scientific Publishing Co.: Singapore, 2002.
(2) Grätzel, M. Solar Energy Conversion by Dye-Sensitized Photovoltaic Cells. *Inorg. Chem.* **2005**, *44*, 6841−6851.
(3) Grätzel, M. Recent Advances in Sensitized Mesoscopic Solar Cells. *Acc. Chem. Res.* **2009**, *42*, 1788−1798.
(4) Hagfeldt, A.; Boschloo, G.; Sun, L. C.; Kloo, L.; Pettersson, H. Dye-Sensitized Solar Cells. *Chem. Rev.* **2010**, *110*, 6595−6663.
(5) Grätzel, M.; Janssen, R. A. J.; Mitzi, D. B.; Sargent, E. H. Materials Interface Engineering for Solution-Processed Photovoltaics. *Nature* **2012**, *488*, 304−312.
(6) Umari, P.; Giacomazzi, L.; De Angelis, F.; Pastore, M.; Baroni, S. Energy-Level Alignment in Organic Dye-Sensitized TiO_2 from GW Calculations. *J. Chem. Phys.* **2013**, *139*, 014709.
(7) Garcia-Lastra, J. M.; Rostgaard, C.; Rubio, A.; Thygesen, K. S. Polarization-Induced Renormalization of Molecular Levels at Metallic and Semiconducting Surfaces. *Phys. Rev. B* **2009**, *80*, 245427.
(8) Garcia-Lastra, J. M.; Rostgaard, C.; Rubio, A.; Thygesen, K. S. Polarization-Induced Renormalization of Molecular Levels at Metallic and Semiconducting Surfaces (vol 80, 245427, 2009). *Phys. Rev. B* **2010**, *81*, 049901.
(9) Garcia-Lastra, J. M.; Thygesen, K. S. Renormalization of Optical Excitations in Molecules Near a Metal Surface. *Phys. Rev. Lett.* **2011**, *106*, 187402.
(10) Thygesen, K. S.; Rubio, A. Renormalization of Molecular Quasiparticle Levels at Metal−Molecule Interfaces: Trends Across Binding Regimes. *Phys. Rev. Lett.* **2009**, *102*, 046802.
(11) Freysoldt, C.; Rinke, P.; Scheffler, M. Controlling Polarization at Insulating Surfaces: Quasiparticle Calculations for Molecules Adsorbed on Insulator Films. *Phys. Rev. Lett.* **2009**, *103*, 056803.
(12) Neaton, J. B.; Hybertsen, M. S.; Louie, S. G. Renormalization of Molecular Electronic Levels at Metal−Molecule Interfaces. *Phys. Rev. Lett.* **2006**, *97*, 216405.
(13) Migani, A.; Mowbray, D. J.; Iacomino, A.; Zhao, J.; Petek, H.; Rubio, A. Level Alignment of a Prototypical Photocatalytic System: Methanol on TiO_2(110). *J. Am. Chem. Soc.* **2013**, *135*, 11429−11432.
(14) Migani, A.; Mowbray, D. J.; Zhao, J.; Petek, H.; Rubio, A. Quasiparticle Level Alignment for Photocatalytic Interfaces. *J. Chem. Theory Comput.* **2014**, *10*, 2103−2113.
(15) Marom, N.; Kim, M.; Chelikowsky, J. R. Structure Selection Based on High Vertical Electron Affinity for TiO_2 Clusters. *Phys. Rev. Lett.* **2012**, *108*, 106801.
(16) Chiodo, L.; Salazar, M.; Romero, A. H.; Laricchia, S.; Sala, F. D.; Rubio, A. Structure, Electronic, and Optical Properties Of TiO_2 Atomic Clusters: An Ab Initio Study. *J. Chem. Phys.* **2011**, *135*, 244704.
(17) Mowbray, D. J.; Martinez, J. I.; Lastra, J. M. G.; Thygesen, K. S.; Jacobsen, K. W. Stability and Electronic Properties of TiO_2 Nanostructures with and without B and N Doping. *J. Phys. Chem. C* **2009**, *113*, 12301−12308.
(18) Hartmann Douma, D.; Gebauer, R. Optical Properties of Dye Sensitized TiO_2 Nanowires from Time-Dependent Density Functional Theory. *Phys. Status Solidi RRL* **2011**, *5*, 259−261.
(19) Brennan, T. P.; Tanskanen, J. T.; Bakke, J. R.; Nguyen, W. H.; Nordlund, D.; Toney, M. F.; McGehee, M. D.; Sellinger, A.; Bent, S. F. Dynamical Orientation of Large Molecules on Oxide Surfaces and Its Implications for Dye-Sensitized Solar Cells. *Chem. Mater.* **2013**, *25*, 4354−4363.
(20) Sai, N.; Leung, K.; Chelikowsky, J. R. Hybrid Density Functional Study of Oligothiophene/ZnO Interface for Photovoltaics. *Phys. Rev. B* **2011**, *83*, 121309.

(21) De Angelis, F.; Fantacci, S.; Selloni, A.; Nazeeruddin, M. K.; Grätzel, M. First-Principles Modeling of the Adsorption Geometry and Electronic Structure of Ru(II) Dyes on Extended TiO_2 Substrates for Dye-Sensitized Solar Cell Applications. *J. Phys. Chem. C* **2010**, *114*, 6054−6061.
(22) De Angelis, F.; Fantacci, S.; Selloni, A.; Grätzel, M.; Nazeeruddin, M. K. Influence of the Sensitizer Adsorption Mode on the Open-Circuit Potential of Dye-Sensitized Solar Cells. *Nano Lett.* **2007**, *7*, 3189−3195.
(23) Nayak, P. K.; Garcia-Belmonte, G.; Kahn, A.; Bisquert, J.; Cahen, D. Photovoltaic Efficiency Limits and Material Disorder. *Energy Environ. Sci.* **2012**, *5*, 6022−6039.
(24) Benedict, J. B.; Coppens, P. The Crystalline Nanocluster Phase as a Medium for Structural and Spectroscopic Studies of Light Absorption of Photosensitizer Dyes on Semiconductor Surfaces. *J. Am. Chem. Soc.* **2010**, *132*, 2938−2944.
(25) Marom, N.; Moussa, J. E.; Ren, X. G.; Tkatchenko, A.; Chelikowsky, J. R. Electronic Structure of Dye-Sensitized TiO_2 Clusters from Many-Body Perturbation Theory. *Phys. Rev. B* **2011**, *84*, 245115.
(26) Blum, V.; Gehrke, R.; Hanke, F.; Havu, P.; Havu, V.; Ren, X.; Reuter, K.; Scheffler, M. Ab Initio Molecular Simulations With Numeric Atom-Centered Orbitals. *Comput. Phys. Commun.* **2009**, *180*, 2175−2196.
(27) Havu, V.; Blum, V.; Havu, P.; Scheffler, M. Efficient O(N) Integration for All-Electron Electronic Structure Calculation Using Numeric Basis Functions. *J. Comput. Phys.* **2009**, *228*, 8367−8379.
(28) Ren, X.; Sanfilipo, A.; Rinke, P.; Wieferink, J.; Tkatchenko, A.; Reuter, K.; Blum, V.; Scheffler, M. An Accurate Resolution of Identity Approach to Hartree-Fock, Hybrid Functionals, MP2, RPA, and GW with Numeric Atom-Centered Basis Functions. *New J. Phys.* **2012**, *14*, 053020.
(29) Perdew, J. P.; Burke, K.; Ernzerhof, M. Generalized Gradient Approximation Made Simple. *Phys. Rev. Lett.* **1996**, *77*, 3865−3868.
(30) Perdew, J. P.; Burke, K.; Ernzerhof, M. Generalized Gradient Approximation Made Simple (vol 77, pg 3865, 1996). *Phys. Rev. Lett.* **1997**, *78*, 1396−1396.
(31) Tkatchenko, A.; Scheffler, M. Accurate Molecular van der Waals Interactions from Ground-State Electron Density and Free-Atom Reference Data. *Phys. Rev. Lett.* **2009**, *102*, 073005.
(32) Hedin, L. New Method For Calculating 1-Particle Green's Function with Application to the Electron-Gas Problem. *Phys. Rev.* **1965**, *139*, A796.
(33) Hybertsen, M. S.; Louie, S. G. Electron Correlation in Semiconductors and Insulators - Band-Gaps and Quasi-Particle Energies. *Phys. Rev. B* **1986**, *34*, 5390−5413.
(34) Onida, G.; Reining, L.; Rubio, A. Electronic Excitations: Density-Functional Versus Many-Body Green's-Function Approaches. *Rev. Mod. Phys.* **2002**, *74*, 601−659.
(35) Marom, N.; Caruso, F.; Ren, X.; Hofmann, O. T.; Körzdörfer, T.; Chelikowsky, J. R.; Rubio, A.; Scheffler, M.; Rinke, P. Benchmark of GW Methods for Azabenzenes. *Phys. Rev. B* **2012**, *86*, 245127.
(36) Jiang, H.; Gomez-Abal, R. I.; Rinke, P.; Scheffler, M. First-Principles Modeling of Localized d States with the GW@LDA+U Approach. *Phys. Rev. B* **2010**, *82*, 045108.
(37) Qteish, A.; Rinke, P.; Scheffler, M.; Neugebauer, J. Exact-Exchange-Based Quasiparticle Energy Calculations for the Band Gap, Effective Masses, and Deformation Potentials of ScN. *Phys. Rev. B* **2006**, *74*, 245208.
(38) Rinke, P.; Qteish, A.; Neugebauer, J.; Freysoldt, C.; Scheffler, M. Combining GW Calculations with Exact-Exchange Density-Functional Theory: An Analysis of Valence-Band Photoemission for Compound Semiconductors. *New J. Phys.* **2005**, *7*, 126.
(39) Rinke, P.; Qteish, A.; Neugebauer, J.; Scheffler, M. Exciting Prospects for Solids: Exact-Exchange Based Functionals Meet Quasiparticle Energy Calculations. *Phys. Status Solidi B* **2008**, *245*, 929−945.
(40) Rinke, P.; Scheffler, M.; Qteish, A.; Winkelnkemper, M.; Bimberg, D.; Neugebauer, J. Band Gap and Band Parameters of InN and GaN from Quasiparticle Energy Calculations Based on Exact-Exchange Density-Functional Theory. *Appl. Phys. Lett.* **2006**, *89*, 161919.
(41) Fuchs, F.; Bechstedt, F. Indium-Oxide Polymorphs from First Principles: Quasiparticle Electronic States. *Phys. Rev. B* **2008**, *77*, 155107.
(42) Rodl, C.; Fuchs, F.; Furthmuller, J.; Bechstedt, F. Quasiparticle Band Structures of the Antiferromagnetic Transition-Metal Oxides MnO, FeO, CoO, and NiO. *Phys. Rev. B* **2009**, *79*, 235114.
(43) Perdew, J. P.; Zunger, A. Self-Interaction Correction to Density-Functional Approximations for Many-Electron Systems. *Phys. Rev. B* **1981**, *23*, 5048−5079.
(44) Körzdörfer, T.; Kümmel, S.; Marom, N.; Kronik, L. When to Trust Photoelectron Spectra from Kohn−Sham Eigenvalues: The Case of Organic Semiconductors. *Phys. Rev. B* **2009**, *79*, 201205.
(45) Körzdörfer, T.; Kümmel, S.; Marom, N.; Kronik, L. When to Trust Photoelectron Spectra from Kohn−Sham Eigenvalues: The Case of Organic Semiconductors (vol 79, 201205, 2009). *Phys. Rev. B* **2010**, *82*, 129903.
(46) Körzdörfer, T. On the Relation Between Orbital-Localization and Self-Interaction Errors in the Density Functional Theory Treatment of Organic Semiconductors. *J. Chem. Phys.* **2011**, *134*, 094111.
(47) Marom, N.; Ren, X. G.; Moussa, J. E.; Chelikowsky, J. R.; Kronik, L. Electronic Structure of Copper Phthalocyanine from G_0W_0 Calculations. *Phys. Rev. B* **2011**, *84*, 195143.
(48) Salomon, E.; Amsalem, P.; Marom, N.; Vondracek, M.; Kronik, L.; Koch, N.; Angot, T. Electronic Structure of CoPc Adsorbed on Ag(100): Evidence for Molecule-Substrate Interaction Mediated by Co 3d Orbitals. *Phys. Rev. B* **2013**, *87*, 075407.
(49) Atalla, V.; Yoon, M.; Caruso, F.; Rinke, P.; Scheffler, M. Hybrid Density Functional Theory Meets Quasiparticle Calculations: A Consistent Electronic Structure Approach. *Phys. Rev. B* **2013**, *88*, 165122.
(50) Körzdörfer, T.; Marom, N. A Strategy for Finding a Reliable Starting Point for G_0W_0 Demonstrated for Molecules. *Phys. Rev. B* **2012**, *86*, 041110(R).
(51) The comparison between different systems, calculated based on functionals with different fractions of exact exchange, is an inherent feature of any electronic structure method containing system dependent parameters [e.g., ref 49; Karolewski, A.; Kronik, L.; Kümmel, S. Using Optimally Tuned Range Separated Hybrid Functionals in Ground-State Calculations: Consequences and Caveats. *J. Chem. Phys.* **2013**, *138*, 204115. Himmetoglu, B.; Floris, A.; de Gironcoli, S.; Cococcioni, M. Hubbard-corrected DFT Energy Functionals: The LDA+U Description of Correlated Systems. *Int. J. Quantum Chem.* **2014**, *114*, 14. Dabo, I.; Ferretti, A.; Poilvert, N.; Li, Y. L.; Marzari, N.; Cococcioni, M. Koopmans' Condition for Density-Functional Theory. *Phys. Rev. B* **2010**, *82*, 115121]. Such comparisons are justified under the assumprion that the system dependent parameters reflect a physical property of the system. In this case, the amount of EXX in the CSP is inversely related to the extent of screening.
(52) Chiodo, L.; Garcia-Lastra, J. M.; Iacomino, A.; Ossicini, S.; Zhao, J.; Petek, H.; Rubio, A. Self-Energy and Excitonic Effects in the Electronic and Optical Properties of TiO_2 Crystalline Phases. *Phys. Rev. B* **2010**, *82*, 045207.
(53) Kang, W.; Hybertsen, M. S. Quasiparticle and Optical Properties of Rutile and Anatase TiO_2. *Phys. Rev. B* **2010**, *82*, 085203.
(54) van Schilfgaarde, M.; Kotani, T.; Faleev, S. Quasiparticle Self-Consistent GW Theory. *Phys. Rev. Lett.* **2006**, *96*, 226402.
(55) Thulin, L.; Guerra, J. Calculations of Strain-Modified Anatase TiO_2 Band Structures. *Phys. Rev. B* **2008**, *77*, 195112.
(56) We note that the GW gaps reported here are larger than the gaps obtained in ref 24 using a hybrid DFT functional. Hybrid functionals do not genrally provide accurate gaps [see: Jain, M.; Chelikowsky, J. R.; Louie, S. G. Reliability of Hybrid Functionals in Predicting Band Gaps. *Phys. Rev. Lett.* **2011**, *107*, 216806]. In some

cases the underestimated gaps obtained with hybrid DFT functionals may fortuitously agree with measured optical gaps.
(57) Sato, N.; Seki, K.; Inokuchi, H. Ultraviolet Photoelectron Spectra of Tetrahalogeno-p-benzoquinones and Hexahalogenobenzenes in the Solid State. *J. Chem. Soc., Faraday Trans. 2* **1981**, *77*, 47−53.
(58) Hill, I. G.; Kahn, A.; Soos, Z. G.; Pascal, J. R. A. Charge-Separation Energy in Films of π-Conjugated Organic Molecules. *Chem. Phys. Lett.* **2000**, *327*, 181−188.
(59) Tkatchenko, A.; DiStasio, R. A., Jr.; Car, R.; Scheffler, M. Accurate and Efficient Method for Many-Body van der Waals Interactions. *Phys. Rev. Lett.* **2012**, *108*, 236402.
(60) Schatschneider, B.; Liang, J.-J.; Reilly, A. M.; Marom, N.; Zhang, G.-X.; Tkatchenko, A. Electrodynamic Response and Stability of Molecular Crystals. *Phys. Rev. B* **2013**, *87*, 060104.
(61) Duncan, W. R.; Prezhdo, O. V. Electronic Structure and Spectra of Catechol and Alizarin in the Gas Phase and Attached to Titanium. *J. Phys. Chem. B* **2005**, *109*, 365−373.
(62) Duncan, W. R.; Prezhdo, O. V. Theoretical Studies of Photoinduced Electron Transfer in Dye-Sensitized TiO_2. *Annu. Rev. Phys. Chem.* **2007**, *58*, 143−184.
(63) Gundlach, L.; Ernstorfer, R.; Willig, F. Ultrafast Interfacial Electron Transfer from the Excited State of Anchored Molecules into a Semiconductor. *Prog. Surf. Sci.* **2007**, *82*, 355−377.
(64) Prezhdo, O. V.; Duncan, W. R.; Prezhdo, V. V. Photoinduced Electron Dynamics at the Chromophore−Semiconductor Interface: A Time-Domain Ab Initio Perspective. *Prog. Surf. Sci.* **2009**, *84*, 30−68.
(65) Redfern, P. C.; Zapol, P.; Curtiss, L. A.; Rajh, T.; Thurnauer, M. C. Computational Studies of Catechol and Water Interactions with Titanium Oxide Nanoparticles. *J. Phys. Chem. B* **2003**, *107*, 11419−11427.
(66) Lundqvist, M. J.; Nilsing, M.; Persson, P.; Lunell, S. DFT Study of Bare and Dye-Sensitized TiO_2 Clusters and Nanocrystals. *Int. J. Quantum Chem.* **2006**, *106*, 3214−3234.
(67) Persson, P.; Bergström, R.; Lunell, S. Quantum Chemical Study of Photoinjection Processes in Dye-Sensitized TiO_2 Nanoparticles. *J. Phys. Chem. B* **2000**, *104*, 10348−10351.
(68) Snoeberger, R. C.; Young, K. J.; Tang, J.; Allen, L. J.; Crabtree, R. H.; Brudvig, G. W.; Coppens, P.; Batista, V. S.; Benedict, J. B. Interfacial Electron Transfer into Functionalized Crystalline Polyoxotitanate Nanoclusters. *J. Am. Chem. Soc.* **2012**, *134*, 8911−8917.